

DECAY CHARACTERISTICS OF SINGLE AND DOUBLE WAKE-VORTEX PAIRS IN DIFFERENT ATMOSPHERIC FLOW REALISATIONS

Thomas Gerz and Robert Baumann

Institut für Physik der Atmosphäre, DLR-Oberpfaffenhofen, 82234 Wessling, D

Keywords: wake vortex, atmosphere, aircraft configuration

Abstract

This study analyses the decay characteristics of aircraft wake vortices as observed in real atmospheric environments. It further assesses the capability and robustness of different wake topologies to trigger quick vortex decays in the atmosphere which, in turn, might alleviate the impact upon encountering aircraft. The analysis focuses on single and double vortex pairs and is based on data from lidar and numerical large-eddy simulations (LES).

1 Introduction

With the global increase of air traffic, the minimum separation distances and times required for wake vortex safety reasons between starting or landing aircraft have become an important capacity limiting factor for major airports. In order to increase airport capacity whilst at least maintaining the safety level of today, the knowledge of wake vortex characterisation and control achieves considerable significance. The possibility that fixed or moving surfaces at the wings and flaps of an aircraft may alleviate the strength of the shed vortices and result in their quicker decay is of utmost importance, especially when designing new large aircraft [1]. Numerical and experimental studies nourish the idea that a system of at least two co- or counter-rotating vortex pairs is required across the symmetry line of the aircraft in the early mid field of the wake to favour the quick growth of unstable modes of the primary vortices [2-5]. Ref. [6] confirms the very unstable nature of some counter-rotating four-vortex configurations by linear stability analysis. Once sufficiently disturbed, the

coherent vortices may decay quickly into incoherent turbulence in the late mid to early far field.

Although proved positively at the laboratory scale by means of experiment, numerics and theory, the capability of such multiple vortex systems to decay fast also at the full scale and in real atmospheric flow conditions yet is an open task. It still has to be demonstrated that the found measures are robust with respect to weather conditions which typically prevail in the atmospheric boundary layer, in particular the ambient turbulence level. Ground-based lidar (light detection and ranging) measurements of aircraft wake vortices so far have shown that the obvious influence of the atmospheric turbulence on the decay of a two-vortex system masks any change in decay rate which may stem from (modestly) different wing or flap configurations at the aircraft [7].

In this study we use the Large-Eddy Simulation (LES) technique [8] to simulate the wake decay as measured by lidar in two campaigns in 2002 and 2003 in South-France in the framework of the European projects *C-Wake* and *AWIATOR*. Once the measured atmospheric state can be reproduced satisfactorily we will quantify the impact of atmospheric turbulence on the vortex decay by parameter variations. Further we simulate the decay of counter-rotating four-vortex systems under such atmospheric conditions and assess the decay characteristics for different background turbulence levels. The goal is to provide guidance for a forthcoming flight test where the trajectory and decay characteristics of a four-vortex system will be measured by an air-borne lidar.

2 Lidar measurements

The primary objective of the WakeTOUL campaign in *C-Wake* and flight-test 1 (F/T-1) in *AWIATOR* was to trace the vortex trajectories and characterise the vortex decay with hitherto unrivalled accuracy under rather calm and neutral atmospheric conditions (“close to laboratory”) for long times. DLR’s WVPMS (wake vortex prediction and monitoring system [9]) has been used to forecast the appropriate weather and wake behaviour in order to plan and guide the over-flights of the aircraft, to monitor the atmospheric parameters, and to measure the wake transport and decay.

A combined sodar and rass system provided 10-minutes averages of profiles of the three wind components and temperature at a vertical resolution of 10-20 m [10]. The typical measurement range was 500 m starting at $z=40$ m. A sonic anemometer with a sampling frequency of 20 Hz was mounted on a 10 m mast close to the sodar/rass. This tool provided turbulence kinetic energy (TKE) spectra from which a turbulent eddy dissipation rate (EDR) at 10 m height could be derived [11]; for larger altitudes TKE and EDR were deduced from the standard variation of the vertical velocity from SODAR scaled by the anemometer value at 10 m. Profiles of cross-wind, TKE and EDR have also been sampled by the pulsed 2 μ m lidar with an averaging window of 5 minutes [12]. This lidar also traced and characterised the wake vortices shed by a large transport aircraft (LTA). The aircraft flew dedicated over-flights with different configurations. Smoke pods mounted on both wings closely at the outer flap edge visualised the vortices and increased the intensity of the light which is backscattered from the aerosols in the vortex to the receiver of the lidar. Fig. 1 sketches the measurement set-up for the lidar and shows an example of a detected wake on the quick-look screen of the lidar.

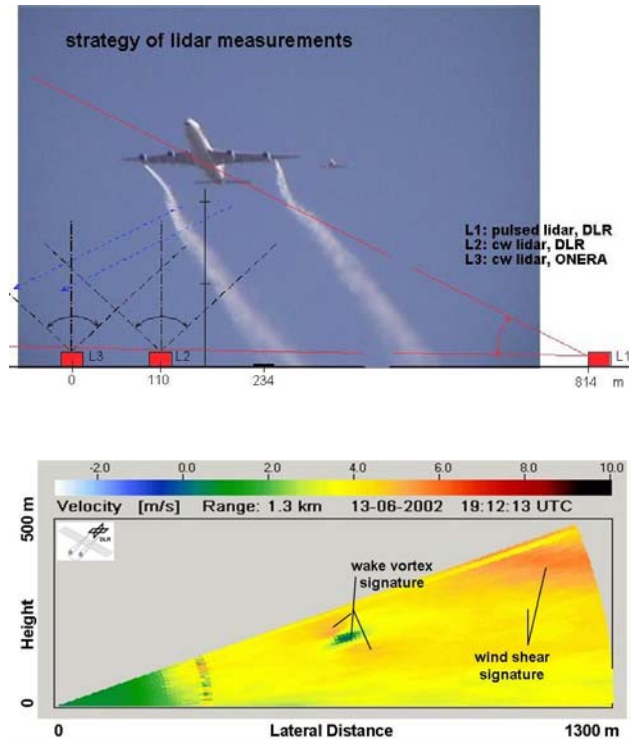


Fig. 1. Top: Measurement strategy in the *C-Wake* (with 3 lidars) and *AWIATOR* campaigns (lidar L1 only). The LIDAR beams crossed the flight path almost perpendicular. The data of the pulsed lidar L1 are analysed in this study. Bottom: Velocity as measured by lidar (quick-look after one scan) with signatures of wind shear and a wake vortex pair.

Fig. 2 (a, b) shows the results of both campaigns in terms of the temporal evolution of the vortex circulation for different atmospheric turbulence levels and different aircraft configurations. The data reveal a relatively large scatter. Nevertheless, the impact of ambient turbulence (see different mean levels of EDR) on the decay of wake vortices is discernible and significant. On the other hand, the (rather slightly) modified flight configurations of the aircraft do not significantly alter the decay rate even under very calm conditions (Fig. 2 c). Three mean values of the dissipation rate have been deduced from the lidar measurements: $\varepsilon = 1, 3, \text{ and } 10 \times 10^{-4} \text{ m}^2\text{s}^{-3}$, labelled as ‘weak’, ‘moderate’ and ‘strong’ turbulence.

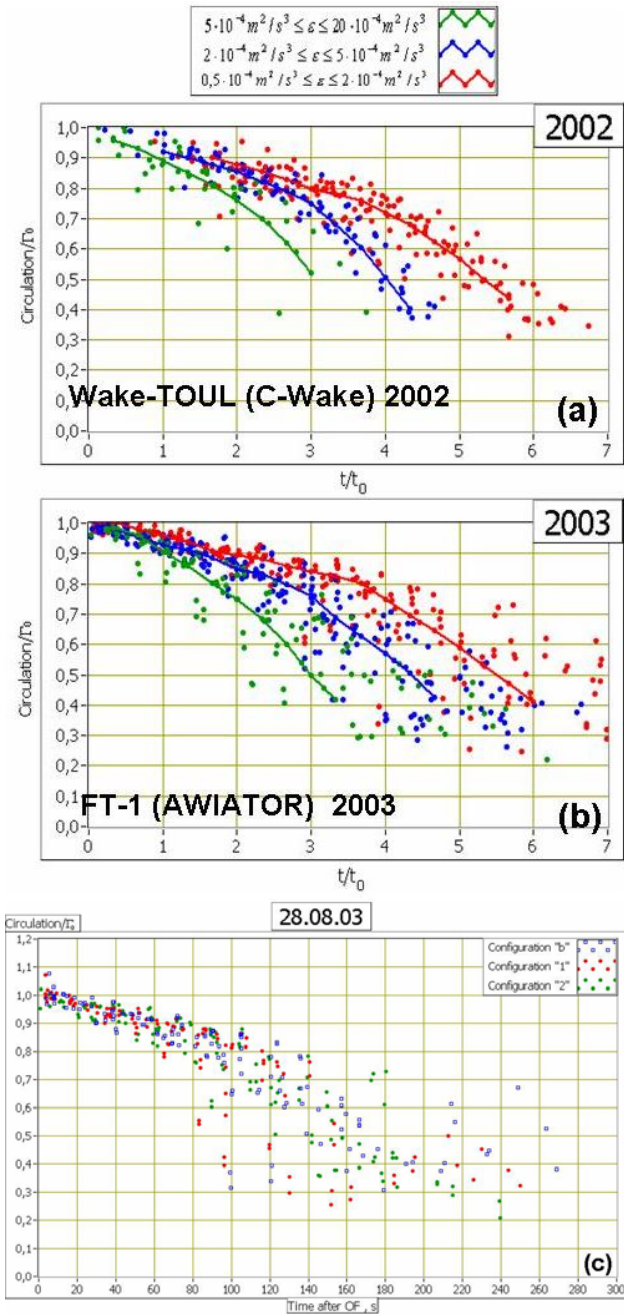


Fig. 2. Vortex circulation versus time as measured by the pulsed lidar. Influence of turbulence (three levels of EDR) for WakeTOUL 2002, 65 over-flights (a) and F/T-1 2003, 32 over-flights (b). Influence of aircraft configuration at the calmest day of F/T-1 (lowest level of EDR), 17 over-flights with 3 modestly different configurations (c). Circulation and time are normalised by the root circulation Γ_0 and the characteristic wake vortex time scale t_0 , respectively.

3 Numerical simulation set-up

For this study of the temporal evolution of the wake vortex flow field in an ambient turbulent atmosphere, we use our three-dimensional, 2nd order finite differences Navier-Stokes solver LESTUF in the large-eddy-simulation (LES) mode [8,13,14]. Unrealistic damping of turbulence in the small vortex core region is reduced by applying the *NaCoo* correction, which is based on local centrifugal stability, to the sub-grid scale viscosity in flow regions of strong streamline curvature [15]. LESTUF implies periodic boundaries in all three directions.

The computational domain is resolved by 480 x 288 x 288 meshes in directions of flight (x), span (y), and altitude (z), respectively, with an isotropic resolution of $\Delta x = \Delta y = \Delta z = 0.8 \text{ m} = r_c/3 = b_0/60$, given an elliptical loading of the wing with span $b=60 \text{ m}$. The terms r_c and b_0 refer to the (initial) vortex core radius and the initial vortex spacing ($b_0 = \pi b/4$). Thus, the domain has a size of 384 x 230.4 x 230.4 m³ or $(8.0 \times 4.8 \times 4.8) b_0^3$. It is considered to be large enough so that spurious effects from the span-wise and vertical boundaries are negligible. The domain extension in flight direction allows the development of the Crow instability.

The vortex core radius r_c is resolved by 3 meshes, i.e. it is 2.4 m or 4% of the wing span; this value is a compromise between the wish to better resolve the vortex core and the attempt to use more realistic, hence, smaller values for r_c . A Burnham-Hallock profile was used as radial velocity profile. On the other hand, the effect of reasonable core radius values on the all-over wake evolution is marginal. Moreover, a realistic treatment of reduced damping of turbulence in the vortex core is guaranteed by the *NaCoo* technique.

In order to obtain realistic background turbulence fields, which resemble the measured atmospheric conditions as close as necessary, a simulation of isotropic turbulence has been performed which produces an almost natural spectral shape ($k^{-5/3}$), and an integral length scale of turbulence L of about 25 m. Fig. 3 shows the (generic) spectra of the three velocity variances and an illustration of the well

developed atmospheric turbulence at the time instant when the vortex pairs will be superimposed to the background flow. The required intensity levels of turbulence (dissipation rates), $\varepsilon = 10^{-6}$, 10^{-4} , and $10^{-3} \text{ m}^2\text{s}^{-3}$, are obtained by adjusting the magnitude of the velocity fluctuations v' according to ε proportional to v'^3/L . The resulting rms values of velocity components, were 0.033 , 0.15 and 0.33 ms^{-1} for $\varepsilon=10^{-6}$, 10^{-4} and $10^{-3} \text{ m}^2\text{s}^{-3}$. The integral length scale of turbulence L and the local flow field topology remain unchanged when adjusting the turbulence level.

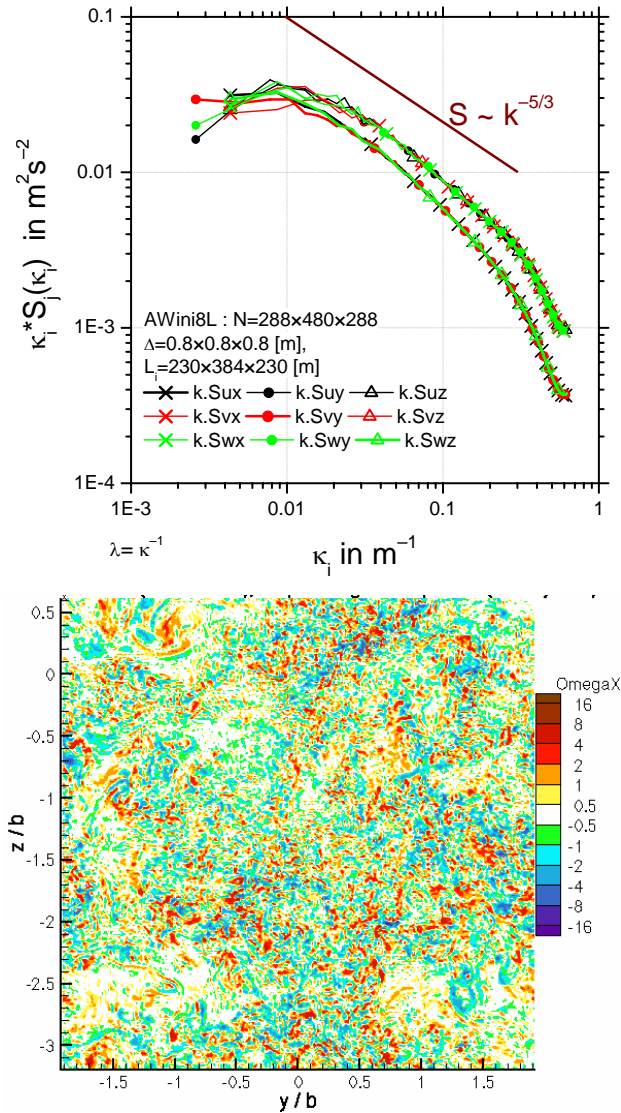


Fig. 3. Directional spectra of the three velocity variances (top, scaled as for $\varepsilon=10^{-3} \text{ m}^2\text{s}^{-3}$) and an illustration of the background turbulence in terms of the vorticity component in flight direction in a y - z -plane (bottom). This flow state has been used to initialise all simulations.

4 Simulation of the measurement scenario

The aircraft wake is represented by a single, rolled-up vortex pair (generic) with circulation $\Gamma_0 = 440 \text{ m}^2/\text{s}$, vortex spacing $b_0 = 48 \text{ m}$, and reference time scale $t_0 = 2\pi b_0^2 \Gamma_0^{-1} = 33 \text{ s}$. The maximum tangential velocity of a single (isolated) vortex at $r = r_c$, V_T , is 14.5 ms^{-1} , the global maximum velocity of the superposition of both vortices is 16 ms^{-1} , due to the induced downwash. We assume that this “generic” wake resembles the real wake of a LTA and superimpose it to the background field as two *laminar* horizontal counter-rotating vortex tubes which extend from $x = 0$ to $x = 384 \text{ m}$.

We perform three wake decay simulations for the values of $\varepsilon = 10^{-6}$, 10^{-4} and $10^{-3} \text{ m}^2\text{s}^{-3}$. The smallest ε value indicates the limiting case where we expect that the effect of the turbulence shed by wing, flaps, jets, and fuselage of the aircraft itself is getting larger than the effect from this very weak background turbulence level. In order to prove this hypothesis, we perform a 4th simulation where the vortex tubes are initialised as *turbulent* vortices in a quiescent atmosphere ($\varepsilon = 0$) [16, 14]. The rationale for the 4th simulation is as follows: Apart from the exhaust mass, also the turbulence from the boundary layer of wing and fuselage as well as the jets are trapped by the wake vortices and the largest turbulence fluctuations are situated around the vortex cores at distance r_c from the centres. In the LES we model the boundary-layer turbulence by adding initially a three-dimensional random perturbation field to the swirling flow such that the perturbation reaches its maximum rms value of 2 m/s at r_c and decays exponentially for smaller and larger radii. This approach is justified as shown in [17] where a laminar flow inside and a turbulent flow just outside the cores of young wingtip vortices has been measured.

We evaluate the circulation by averaging over radii between 5 and 15 m,

$$\Gamma_{5-15} = \frac{1}{11} \sum_{i=5}^{15} \Gamma(i), \quad \text{where } \Gamma(i) = \iint_{r \leq i[m]} \omega_x \, dy \, dz$$

with radius $r = \sqrt{(y - y_c)^2 + (z - z_c)^2}$ and the

$$\text{centroid } y_c = \frac{\iint_A y \omega_x dydz}{\iint_A \omega_x dydz}, \quad z_c = \frac{\iint_A z \omega_x dydz}{\iint_A \omega_x dydz}$$

as the appropriate parameters for encounter severity and lidar data comparison. In the double integrals defining the centroid position, “A” denotes the area containing only the strongest vortex within one half of the y-z-plane. Γ_{5-15} is then analysed as a function of the position along the x-axis and simulation time t.

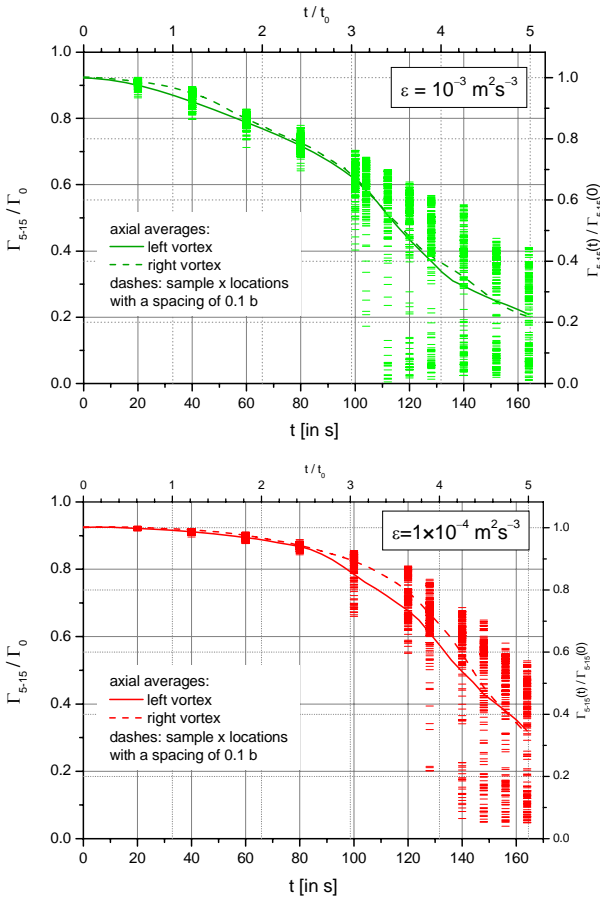


Fig. 4. Decay of the simulated 2-vortex system: Axial mean $\Gamma_{5-15}(t)$ (averaged along local vortex axis at constant age) and its scatter (example values at an arbitrary plane perpendicular to the flight direction for a given vortex age) for two atmospheric eddy dissipation rates $\varepsilon=10^{-3}$ (top) and $10^{-4} \text{ m}^2\text{s}^{-3}$ (bottom).

Fig. 4 depicts the decay of vortex strength in terms of Γ_{5-15} for two levels of background turbulence. The thick lines represent averages along the x-axis, while the small horizontal bars illustrate the scatter for individual y-z-planes at

the given time. A two-phase decay is clearly discernible. The high scatter after the onset of rapid decay is also evident. It is noteworthy that the simulations reproduce the strongly scattering lidar data: after linking portions of the wake exist with still high level of intensity and at the same time but at different axial positions the wake has ceased to zero circulation. This large scatter is also reflected in Fig. 5. One may observe a rapid decay of local circulation at the position where the two vortices link after 104 s (128 s) for $\varepsilon=10^{-3}$ (10^{-4}) m^2s^{-3} , see also Fig. 8 (left panel). From that linking position the circulation increases gradually to both sides.

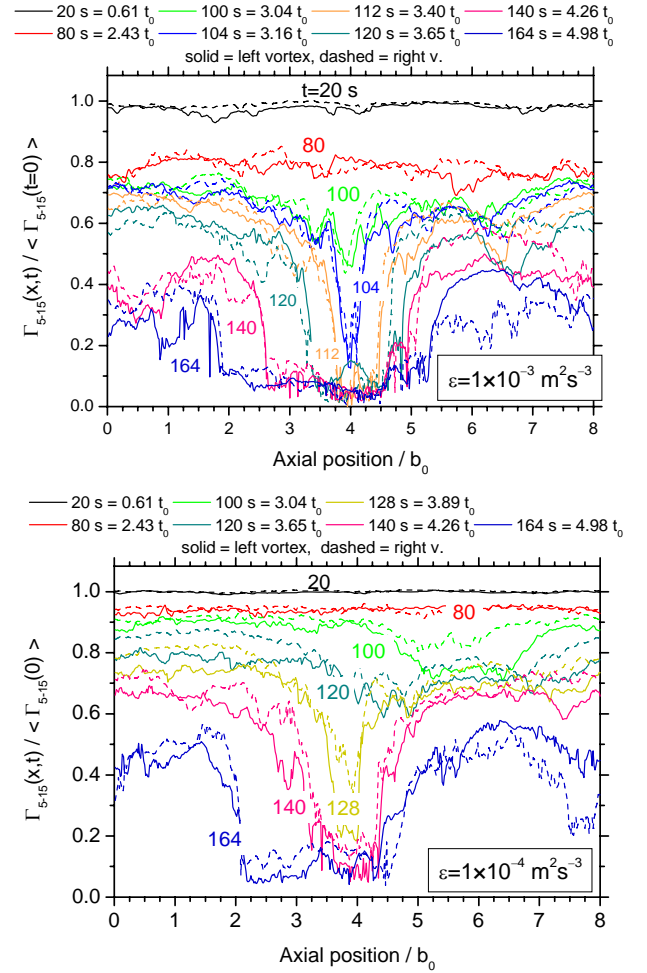


Fig. 5. Decay of a 2-vortex system along the axial position: local variation of $\Gamma_{5-15}(x,t)$; $\varepsilon = 10^{-3}$ (top), $\varepsilon=10^{-4} \text{ m}^2\text{s}^{-3}$ (bottom).

Fig. 6 compares the simulation results with the lidar mean and individual data. The accordance between LIDAR and LES data is very good for the case with mean $\varepsilon=10^{-3} \text{ m}^2\text{s}^{-3}$ whereas for the

weaker background flow ($\varepsilon=10^{-4} \text{ m}^2\text{s}^{-3}$) the simulated wake decays somewhat faster than in the plane observed by the lidar. It should be noted that a lidar overestimates the circulation at late times when the vortices erode and deform quickly such that smaller circulation values cannot be detected unambiguously from ambient turbulence.

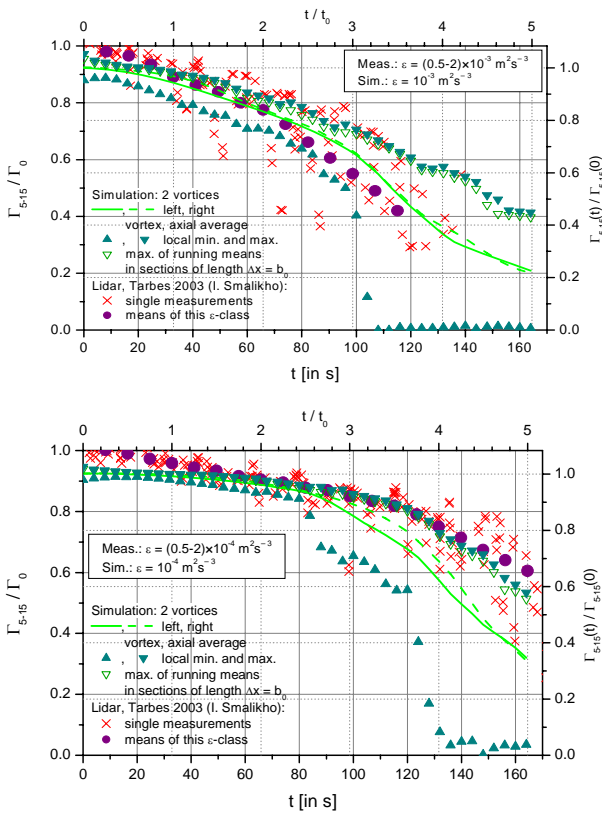


Fig. 6. Comparison of simulated and observed wake decay including LES maxima and minima and the measurement data, $\varepsilon = 10^{-3}$ (top), $\varepsilon=10^{-4} \text{ m}^2\text{s}^{-3}$ (bottom).

5 Simulation of counter-rotating vortex pairs

Now we assess the decay properties and robustness of two counter-rotating vortex pairs imposed on an atmosphere as, e.g., measured during both flight campaigns. Numerous laboratory (e.g. [18, 19]) and CFD studies [20-22] indicate that such a 4-vortex system as sketched in Fig. 7 is capable to trigger an enhanced decay and to alleviate the reactions of aircraft possibly encountering such a wake.

The aircraft wake is represented by two, rolled-up, counter-rotating, (generic) vortex pairs with circulation ratio $\Gamma_2 / \Gamma_1 = -0.35$, vortex spacing ratio $b_2 / b_1 = 0.35$, and the same total lift as for the 2-vortex system $\Gamma_0 b_1 = \Gamma_1 b_1 + \Gamma_2 b_2$, hence $\Gamma_1 = 1.14 \Gamma_0$. The maximum tangential velocity (of one isolated vortex) at $r = r_c$, V_T , is 16.6 ms^{-1} , the global maximum velocity of the vortex flow is 19.4 ms^{-1} . The vortex-induced velocity field is superimposed on the same background flow as described in section 4.

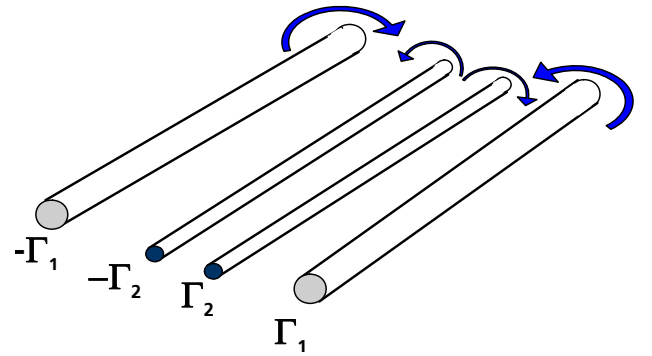
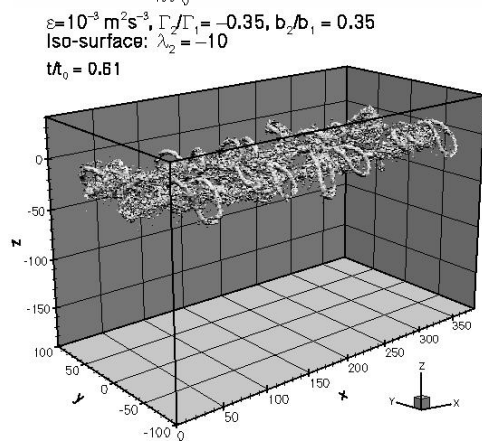
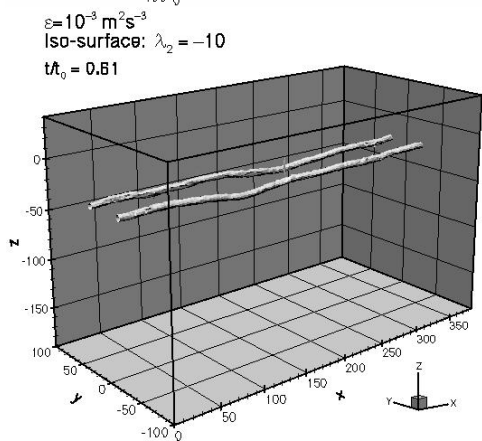
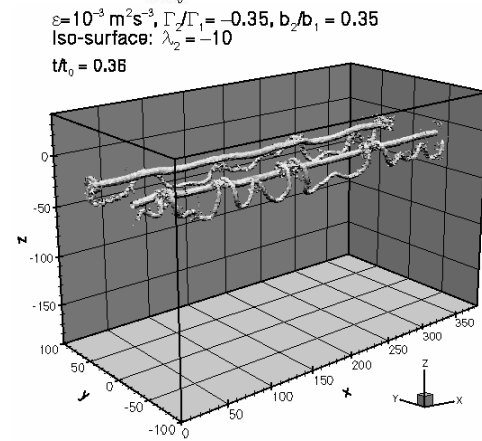
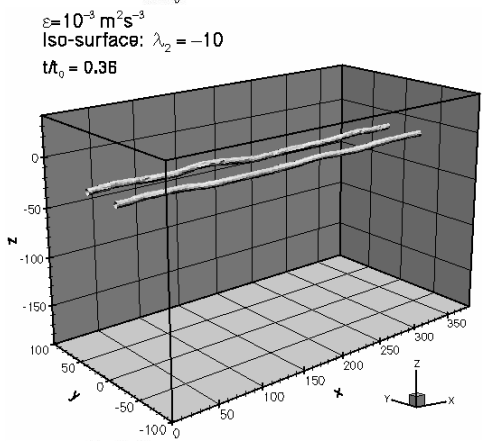
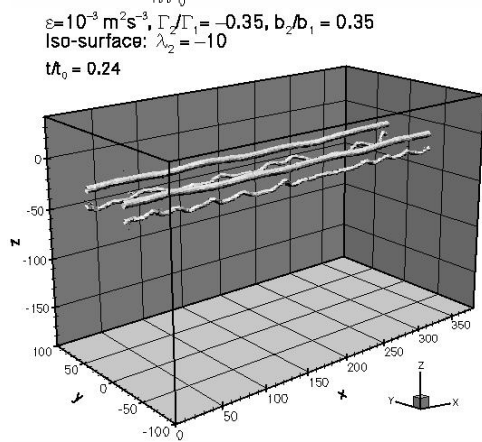
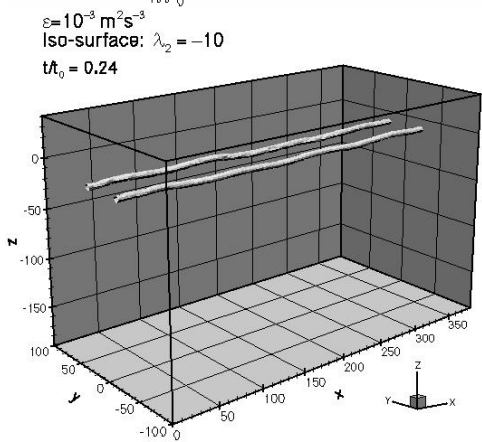
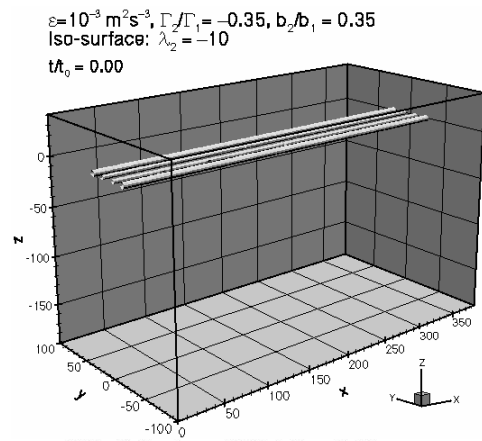
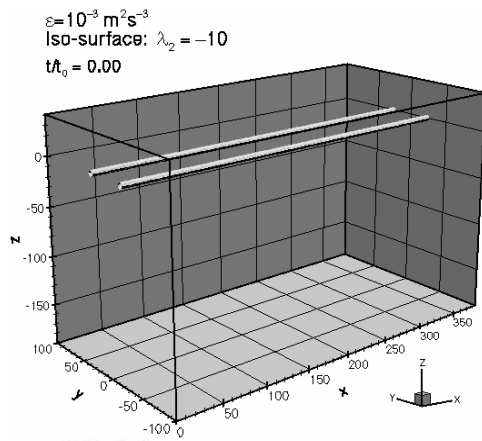


Fig. 7. Sketch of an initial configuration of a 4-vortex system here described by $\Gamma_2 / \Gamma_1 = -0.35$ and $b_2 / b_1 = 0.35$; Index 2 (1) denotes circulation and spacing of the inner (outer) vortex pair.

Fig. 8 shows the evolution of the vortex structures in a perspective view for the 2-vortex and 4-vortex cases in an environment characterised by $\varepsilon=10^{-3} \text{ m}^2\text{s}^{-3}$. In the 2-vortex system disturbances forced by the atmospheric flow grow relatively slowly, leading to a linking at about $t/t_0 = 3$. In contrast, the weaker, initially inner vortices of the 4-vortex system start to distort very early (clearly visible already at $t/t_0=0.24$), forming Ω -shaped loops which touch the main vortices at or before $t/t_0=0.36$. At $t/t_0 \approx 1$ some parts of the loops already have been closed to independent ovals which quickly drift away from the main pair and/or dissolve. After $t/t_0 \approx 2$ only two, strongly distorted vortices remain visible.

DECAY CHARACTERISTICS OF WAKE-VORTEX PAIRS IN DIFFERENT ATMOSPHERIC FLOW REALISATIONS



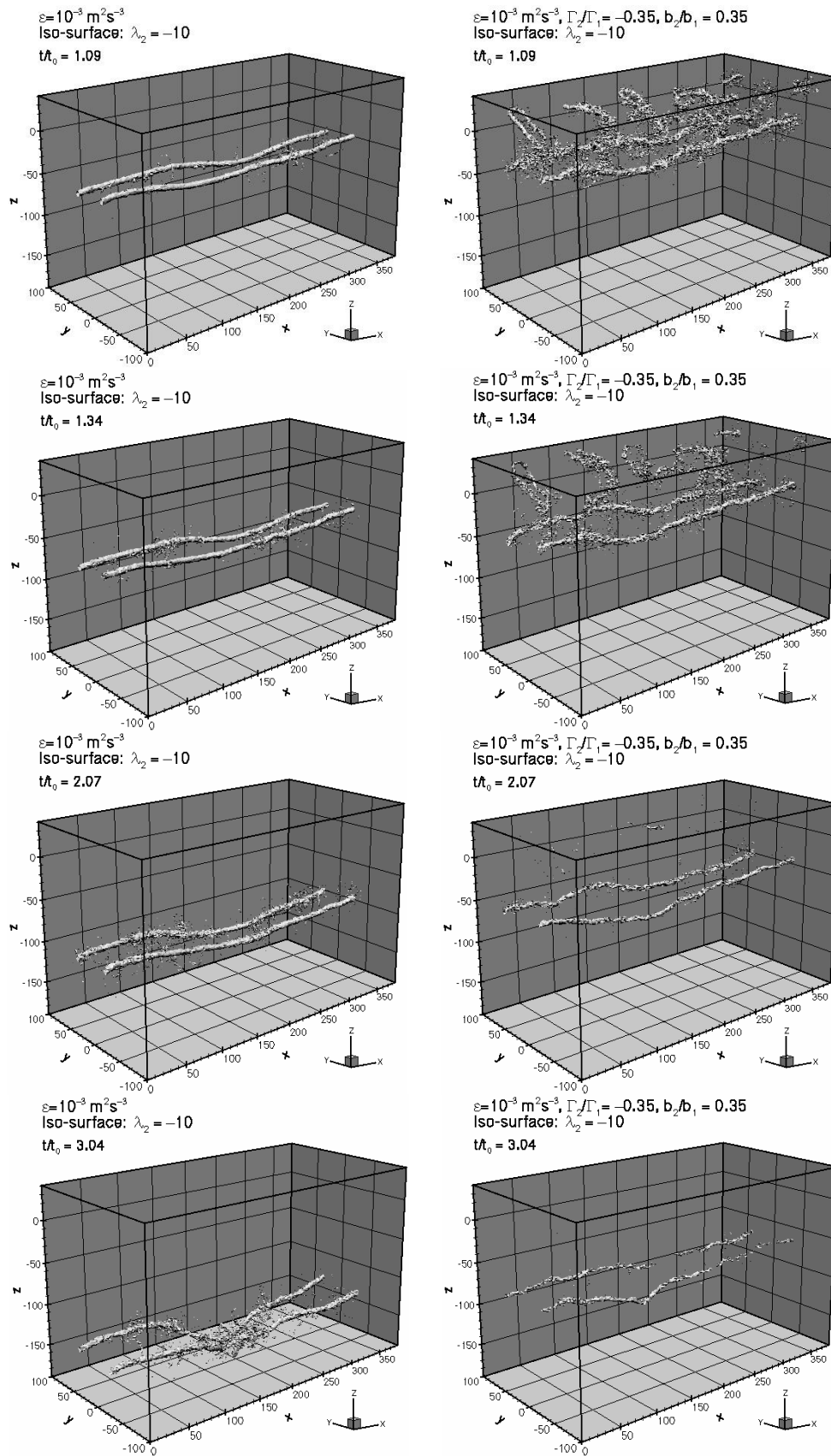


Fig. 8. Development of a 2-vortex system (left) and a 4-vortex system (right) at instances of time $t/t_0 = 0$ through 3.04. The ambient turbulence level is $\varepsilon=10^{-3} \text{ m}^2/\text{s}^3$. Iso-surfaces of λ_2 (a measure of turbulence coherence) are shown.

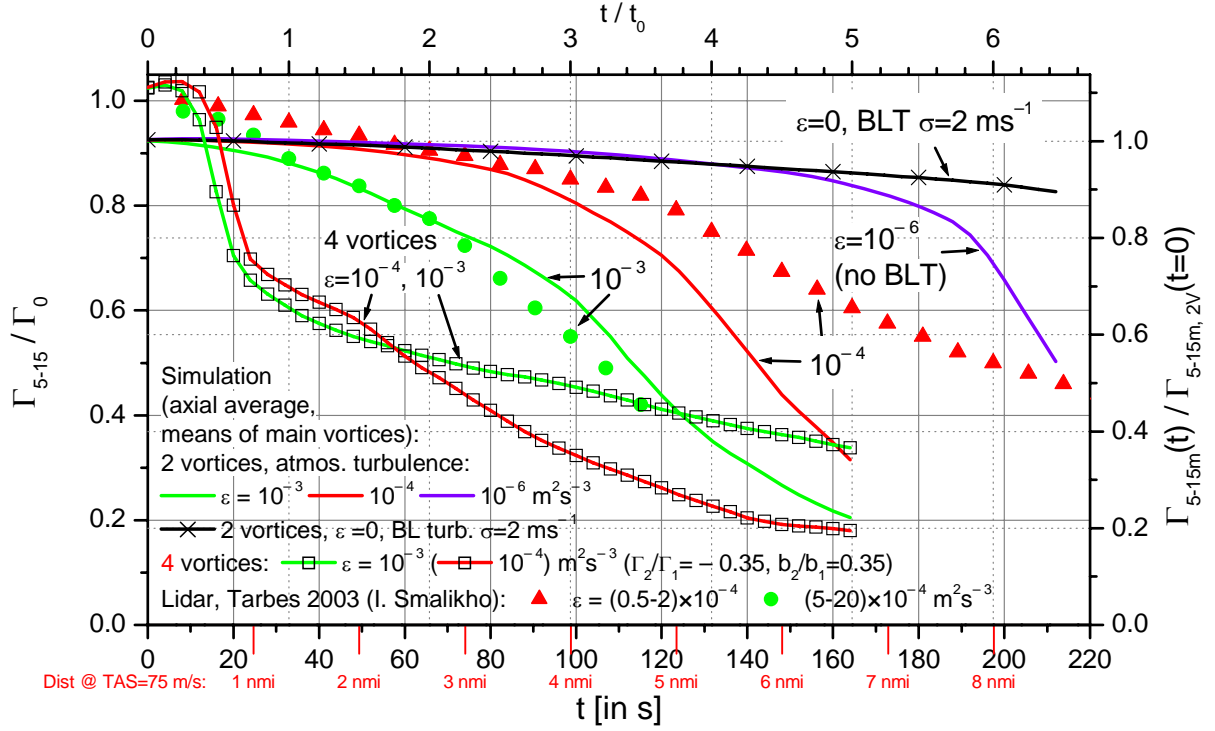


Fig. 9. Axial mean Γ_{5-15} (averaged along local vortex axis at constant age), for different configurations and background turbulence levels. Note: Γ_0 refers to the 2-vortex configuration with equal total lift. Distance axis (red) scaled for true airspeed $V_0=75$ m/s. BLT = entrained boundary layer turbulence.

The qualitative impression from Fig. 8 is that at the end, the (initial) 4-vortex system produces a weaker and less coherent wake topology compared to the 2-vortex system. This qualitative impression is confirmed also quantitatively in Fig. 9. In that figure all mean circulation results of the performed LES are depicted for completeness, i.e. the circulation evolutions are shown for the 2-vortex cases with $\varepsilon=10^{-3}$, 10^{-4} , 10^{-6} , and $0 \text{ m}^2\text{s}^{-3}$, where the last case assumes a turbulence which stems from the boundary layer of the aircraft and is wrapped around the vortex cores. Also shown are the 4-vortex cases with $\varepsilon=10^{-3}$ and $10^{-4} \text{ m}^2\text{s}^{-3}$ as well as the mean Γ_{5-15} values deduced from the lidar measurements. Fig. 9 illustrates that for the 4-vortex system, the circulation, although initially higher to compensate for the reduced lift imposed by the counter-rotating inner vortex pair, decays rapidly to about 60 % of Γ_0 after one reference time scale only.

Even more remarkable is the different influence of the atmospheric turbulence level. While in the 4-vortex configuration the ambient

turbulence level does not significantly alter that rapid decay, the decay of the 2-vortex system is very sensitive to the eddy dissipation rate (and even to local topology of the background field). Decreasing the eddy dissipation ε essentially shifts the time of the onset of rapid decay to later times. This shift is approximately proportional to the logarithm of $1/\varepsilon$: lowering ε by a factor of 10 shifts the onset of rapid decay by approximately $1 \pm 0.2 t_0$.

Surprisingly, the curves for the 4-vortex systems cross at $t/t_0 \approx 1.8$ (≈ 60 s). This behaviour is not yet well understood, but probably it has to do with the spacing of the main vortices which oscillates in a multiple vortex system since the vortices rotate around the common centroid. The level of turbulence determines the time at which the distortions due to short-wave instabilities have reached a certain level at which merging is triggered. Thus, the background turbulence determines the spacing at the time of the first rapid decay in a multi-vortex system. This may, in consequence, alter the further decay history as seen in that example.

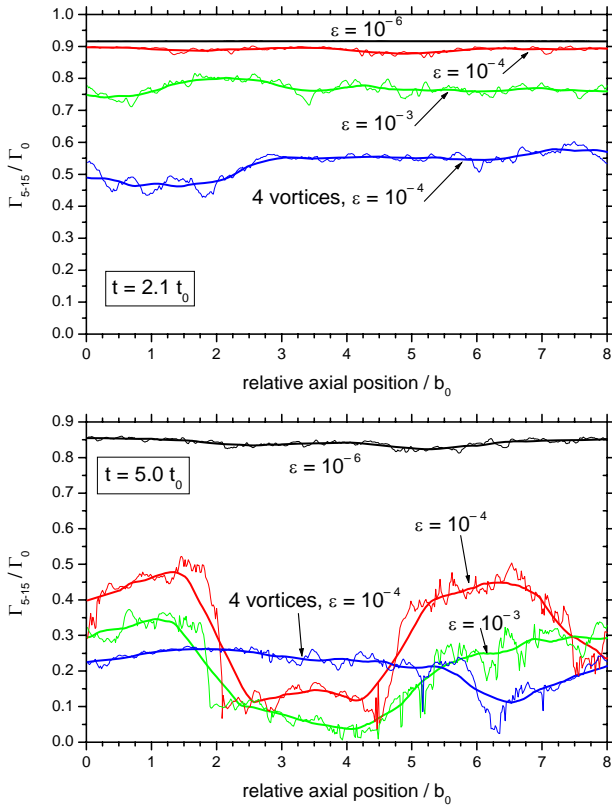


Fig. 10. Decay of a circulation Γ_{5-15} along the axial position. Comparison of different configurations (blue curves: 4-vortex system, others: 2-vortex system) and background turbulence levels at $t/t_0 = 2.1$ (top) and 5.0 (bottom). Shown are local values of Γ_{5-15} and running averages (thicker curves, averaging lag is b_0).

Fig. 10 compares the *local* circulation in different atmospheric conditions and for wake topologies in a view along the x-(flight) axis at two instants of time. This plot indicates how quickly the vortices loose their alignment along the flight path and hence, how quickly the potential hazard fades away when an aircraft encounters that wake.

Similar as the circulation, also the kinetic energy of the wake is decaying very quickly for the 4-vortex system, as shown in Fig. 11. The total kinetic energy, per unit length of the vortex axis, can be expressed as

$$E_{kin} = \frac{1}{2L_x} \sum_{i=1}^3 \iiint u_i^2 dx dy dz.$$

A quantity, which especially pronounces the decay of ordered, rotational flow in a plane perpendicular to the flight-axis is that part of the kinetic energy, which is calculated from the

axially averaged velocity components only. It is defined by

$$E_{avg} = \frac{1}{2} \sum_{i=1}^3 \iint (\bar{u}_i)^2 dy dz \quad \text{with} \quad \bar{u}_i = \frac{1}{L_x} \int_0^{L_x} u_i dx.$$

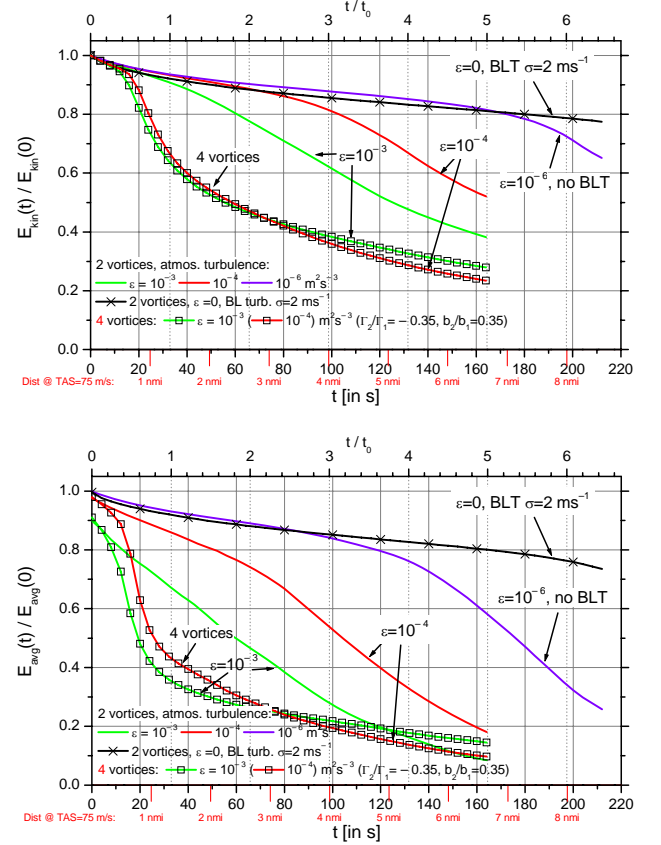


Fig. 11. Kinetic energy normalised with the initial value, cases as in Fig. 9. Top: E_{kin} of the resolved flow, bottom: averaged 2D flow energy E_{avg} .

Fig 11 (bottom) displays this 2D flow energy. The difference $E_{kin} - E_{avg}$ is a measure of the 3-dimensionality, or the transition of coherent flow into turbulent flow. At $t=0$ the difference is simply the energy of the atmospheric background flow. For $\varepsilon=10^{-3} \text{ m}^2 \text{ s}^{-3}$ the total kinetic energy of the background flow is about 11% of the total kinetic energy contained in the vortex flow. (Note, however, that this number is the average for the whole computational domain, whereas at the location of the vortex cores, the atmospheric contribution to energy density is almost vanishing: $3\sigma^2 / V_T^2 \approx 1.5 \times 10^{-3}$ (cf. Sections 3 and 4).

From Fig. 8 we may observe that the interaction between primary and secondary vortices of the double vortex pair is completed roughly

around $t = 2t_0$. At that time a single and highly disordered vortex pair is left with energy levels below $E_{kin} = 0.5 E_{kin}(0)$ and $E_{avg} = 0.3 E_{avg}(0)$, respectively (Fig. 11). This result is corroborated by computations with a spectral code [22]. There the flow was triggered by small random perturbations (‘white noise’) in contrast to our simulations with a ‘red’ background spectrum (Fig. 3). The interaction in [22] was found to be completed around $t = 3_0$ with $E_{kin} = 0.3 E_{kin}(0)$ and $E_{avg} = 0.2 E_{avg}(0)$, respectively.

For the simulated case with $\varepsilon = 10^{-6} \text{ m}^2 \text{ s}^{-3}$ we observe an energy drop of about 10% within the first 60 seconds. This decay in an almost quiet environment is partly due to numerical diffusion of the maximum tangential velocity at the core radius – recall that the core radius is only coarsely resolved by 3 meshes. On the other hand, the artificial diffusion does not affect the averaged circulation Γ_{5-15} (Fig. 9). The performance of a second-order finite difference scheme has been analysed in a benchmark study of different CFD codes [23]. There it was concluded that in the context of aircraft wakes and their evolution in the atmosphere, any turbulent background flow or other superimposed turbulence source will supersede the numerical noise of the code. This is shown in Fig. 11 by comparing the case $\varepsilon = 10^{-6} \text{ m}^2 \text{ s}^{-3}$ (no boundary-layer turbulence) with the cases $\varepsilon = 0$ (with BLT) or $\varepsilon = 10^{-4} \text{ m}^2 \text{ s}^{-3}$. Moreover, much more than numerical diffusion will the local properties of the background flow impact the wake decay, as will be discussed next.

Obviously, the interaction of the vortices of the 4-vortex system creates its own turbulent environment; it just needs to be ‘kicked-off’ by some disturbance of the background flow. This interpretation is corroborated by further simulations where we created a locally different background flow state (flow topology) by changing the set of random numbers. Both flow states have similar global statistics (variances, spectra, integral length scale) and (exactly) the same ‘global’ eddy dissipation rate. Again, the evolution of the 4-vortex system is hardly affected by the different flow topologies whereas the evolution of the 2-vortex system

changes in terms of the onset of the rapid decay and the decay rate of Γ . When we instead place the single vortex pair at another location in the identical background flow we observe differences in the flow evolution after $t > 3.5 t_0$ corresponding to about 5 nautical miles.

The sensitivity to local topology may be explained by the excitation of different modes of distortion due to locally different spectral power of the atmospheric turbulence. Fig. 12 demonstrates this in a top view to the vortex pair. It can be seen, that in the atmospheric case #2 essentially a wave with half the wavelength as in #1 dominates the distortion, leading to faster linkage and destruction of the vortices.

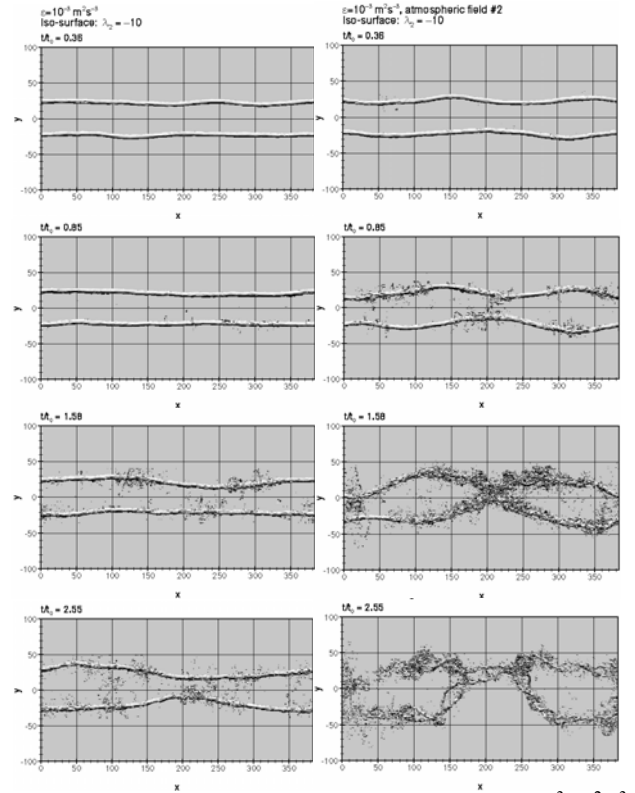


Fig. 12. Evolution of the 2-vortex system at $\varepsilon = 10^{-3} \text{ m}^2 \text{ s}^{-3}$ for two locally distinct atmospheric background flow realisations #1 (left) and #2 (right).

The interaction of the secondary with the primary vortices in a counter-rotating 4-vortex system also leads to variations of the vortex spacing. The revolution of the inner vortices first below and then outwards of the primary vortices (cf. Fig. 8) increases the spacing of the latter and reduces the descent speed of the system. After a full revolution (without linking)

the spacing would be reduced again and the descent speed would have recovered to the initial value. Hence, the time of linkage between the secondary with primary vortices within the revolution cycle determines and freezes the spacing and descent speed and, moreover, alters the characteristic time scale. This effect is demonstrated in Fig. 13: The spacing of the primary vortices of the 4-vortex system increases to about $1.5 b_0$ after $0.5 t_0$ and then the secondary vortices link with the primary ones (cf. Fig. 8). This results in a transient stall of the vortex system and eventually in a reduced descent rate at increased vortex spacing. In consequence, the characteristic time scale has more than doubled compared to a classical vortex pair (2 vortices) where we observe a sink and spacing behaviour according to theory. In conclusion, a reduction in circulation and coherence/alignment of the 4-vortex system is paid by larger spacing and reduced sink speed.

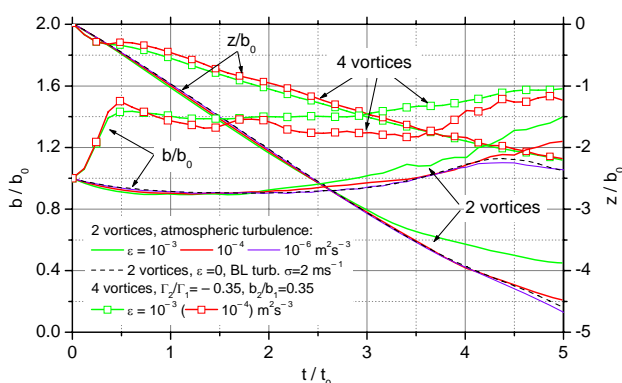


Fig. 13. Effect of wake topology and atmospheric eddy dissipation rate on mean spacing (left ordinate) and descent height (right ordinate) of the vortices. Here: b =spacing of main vortex pair, b_0 = initial spacing of main vortex pair = b_1 , z =vertical position relative to vortex generation.

8 Conclusions

This study showed that LES can reasonably well reproduce lidar measurements of wake vortex decay in atmospheric conditions which are described primarily by the dissipation rate of turbulence kinetic energy. The simulated scatter is consistent with and can explain the measured scatter. Single vortex pairs develop a long-wave (Crow) instability which depends on realised

flow topology. The onset of rapid decay for this wake varies by roughly $1.5 t_0$ depending on local impact of the background flow. Double (counter-rotating) vortex pairs develop a transient medium-wave instability of size b_0 . This instability of the counter-rotating vortex pair is robust with respect to background flow realisation (intensity and topology), since it produces ‘its own’ turbulence.

Acknowledgements

The comments by two reviewers, Anton de Bruin and Grégoire Winckelmans are highly appreciated. Parts of this work are funded by the European Commission under contract G4RD-CT-2002-00836, Project AWIATOR.

References

- [1] Rossow V J. Lift-generated vortex wakes of subsonic transport aircraft. *Prog. Aerosp. Sci.* **35**, pp 507-660, 1999.
- [2] Crouch J D. Instability and transient growth for two trailing-vortex pairs. *J. Fluid Mech.* **350**, pp 311–330, 1997.
- [3] Spalart P R. Airplane trailing vortices. *Annu. Rev. Fluid Mech.* **30**, pp 107 – 138, 1998.
- [4] Gerz T, Holzäpfel F, Darracq D. Commercial aircraft wake vortices. *Prog. Aerosp. Sci.* **38**, pp 181-208, 2002.
- [5] Jacquin L, Fabre D, Sipp D, Theofilis V, Vollmers H. Instability and unsteadiness of aircraft wake vortices. *Aerosp. Sci. Tech.* **7**, pp 577-593, 2003.
- [6] Fabre D, Jacquin L, Loof A. Optimal perturbations in a four-vortex aircraft wake in counter-rotating configuration. *J. Fluid Mech.* **451**, pp 319–328, 2002.
- [7] Köpp F, Rahm S, Smalikho I, Dolfi A, Cariou J-P, Harris M, Young R. Comparison of wake-vortex parameters measured by pulsed and continuous-wave lidars. *J. Aircraft*, **42**, No.4, pp 916-923, 2005.
- [8] Baumann R, Gerz T. Large-eddy simulations of two disturbed counter-rotating vortex pairs. *Proc. EUROMECH Colloquium No 443 Dynamics of Trailing Vortices*, Aachen, pp 1-3, 2002.
- [9] Gerz T, Tafferner A, Rosczyk S, Mirza A, Turp D, Le Bot Ch. Improved weather information for cockpit and tower. *Proc 25th International Congress of the Aeronautical Sciences*, Hamburg, pp 1-13, 2006.
- [10] Gerz T, Holzäpfel F, Bryant W, Köpp F, Frech M, Tafferner A, Winckelmans G. Research towards a wake-vortex advisory system for optimal aircraft

- spacing. *Comptes Rendus Physique, Académie des Sciences, Paris*, Vol. 6, No 4-5, pp 501-523, 2005.
- [11] Frech M. Estimating the turbulence energy dissipation rate in an airport environment. Sub. to *Boundary Layer Meteorology*, 2006.
- [12] Smalikho I, Köpp F, Rahm S. Measurement of atmospheric turbulence by 2- μ m Doppler lidar. *J. Atmos. Oceanic Techn.* Vol. 22, pp 1733 -1747, 2005.
- [13] Holzäpfel F, Gerz T, Frech M, Dörnbrack A. Wake vortices in a convective boundary layer and their influence on following aircraft. *J. Aircraft* 37, No. 6, pp 1001-1007, 2000.
- [14] Holzäpfel F, Gerz T, Baumann R. The turbulent decay of trailing vortex pairs in stably stratified environments. *Aerosp. Sci. Technol.* Vol. 5, pp 95-108, 2001.
- [15] Holzäpfel F. Adjustment of subgrid-scale parametrizations to strong streamline curvature. *AIAA-J* 42 No. 7, pp 1369-1377, 2004.
- [16] Gerz T, Holzäpfel F. Wingtip vortices, turbulence, and the distribution of emissions. *AIAA J.* 37 No. 10, 1270-1276, 1999.
- [17] Devenport W J, Zsoldos J S, Vogel C M. The structure and development of a counter-rotating wing-tip vortex pair. *J. Fluid Mech.* 332, pp 71-104, 1997.
- [18] Bristol R L, Ortega J M, Marcus P S, Savas Ö. On cooperative instabilities of parallel vortex pairs. *J. Fluid Mech.*, 517, pp. 331-358, 2004.
- [19] Savas Ö. Experimental investigations on wake vortices and their alleviation. *Comptes Rendus Physique, Académie des Sciences, Paris*, Vol. 6, No 4-5, 2005.
- [20] Stumpf E. Study of four-vortex aircraft wakes and layout of corresponding aircraft configurations, *J. Aircraft*, 42, No 3, pp 722-730, 2005.
- [21] Winckelmans G, Cocle R, Dufresne L, Capart R. Vortex methods and their application to trailing wake vortex simulations. *Comptes Rendus Physique, Académie des Sciences, Paris*, Vol. 6, No 4-5, pp 467-486, 2005.
- [22] Dufresne L, Winckelmans G, Capart R. LES of instabilities, vortex reconnection and global decay of counter-rotating four-vortex systems. *Proc. Wakenet2-Europe Workshop*, Toulouse, 2005.
- [23] Dufresne L, Capart R, Winckelmans G. Report of benchmark study: Large-eddy simulation of wake vortex flows at very high Reynolds numbers; a comparison of different methodologies. *AWIATOR Report D1.1.4-16*, 2005.